Study of an Ultrawideband Monopole Antenna With a Band-Notched Open-Looped Resonator

Sung-Jung Wu, Cheng-Hung Kang, Keng-Hsien Chen, and Jenn-Hwan Tarng, *Senior Member, IEEE*

***Abstract*—A novel band-notched planar monopole ultrawideband (UWB) antenna is proposed. A notched band, located in the 5 GHz WLAN band, is created using a resonator at the center of a fork-shaped antenna. The resonator is composed of an open-looped resonator and two tapped lines. With the open-looped resonator, the antenna has a good band-notched performance and bandstop-filter-like response in the target band. A parametric study of the notched bandwidth is described that explored the antenna operating mechanism. Then, an equivalent circuit model illustrates the band-notched behaviors more clearly. The antenna input admittance calculated with the equivalent circuit model reasonably agrees with the HFSS simulated result. The proposed antenna also features flat gain frequency responses, small varied group delay and 15 to 35 dB gain suppression at the notched band. Accordingly, the band-notched antenna can effectively select target bands by adjusting these antenna parameters.**

***Index Terms*—Equivalent circuits, high quality factor, monopole antenna, open-looped resonator, ultrawideband (UWB) antenna.**

I. Introduction

In 2002, the Federal Communication Commission (FCC) officially assigned an unlicensed 3.1–10.6 GHz bandwidth with less than -41.3 dBm/MHz effective isotropic radiated power (EIRP) level for commercial applications of ultrawideband (UWB) systems. In this regulated signal condition, UWB technology is applied in extremely high transmission rates over a short distance, i.e., 480 Mbps data rate signal over 10 m transmission distance [1], [2].

Many studies have proposed an extreme broadband antenna for UWB radio systems [3]–[10]. Abbosh *et al.* discussed the performances of UWB planar monopole antennas with a circular or elliptical shape [5]. Chen *et al.* discussed ground plane effect on a small print UWB antenna [6]. Cheng *et al.* proposed a compact and low profile printed wide-slot inverted cone antenna for UWB applications [7]. Low *et al.* described a UWB suspended plate antenna (SPA) with enhanced impedance and radiation performance [9].

Over the inherently operating bandwidth of the UWB system, the existing bands are used by a wireless local-area network (WLAN). Therefore, the UWB antenna with a band-notched characteristic is required to reduce the interference. Researches in some literatures produce band-rejection characteristics by cutting a slot on the antenna [11]–[14] or adding a tuning metal stub within the antenna structure [15], [16]. Several researchers have created transmission zero at the required notched bands by introducing associated resonators in the antenna. By placing the resonator in the antenna, the antenna impedance shifts to a very high or very low level and brings out impedance mismatch at the notch band. Simultaneously, the antenna at notched band is similar to the virtual-open or virtual-short circuit and is capable of not only preventing energy from transmitting to free space, but of also avoiding receiving the unwanted signal from free space. Qu *et al.* created a notched band by a coplanar waveguide resonant cell [17]. Zaker *et al.* used an H-shaped conductor-backed plane to generate band-notched effect [18]. Other resonator forms, such as folded strips, two T-shaped stubs and capacitive-load strips have also been applied for band-notching purposes [19]–[21].

Although the resonators are well accepted in band-notched antenna design, band-notched antenna performance is sometimes quite limited owing to the structure of the antenna and resonator. Meanwhile, the return loss level at the notched band is also a crucial factor for estimating gain suppression. In general, the return loss level is simply in reverse proportion to the gain suppression of the antenna. The following examples explain the limited performance. The first example is that the amount of gain suppression is around 20 dB at specific angles, but the gain suppression is only several dB at $\theta = 0^\circ$ [19]. The next example is that the bandwidth of the notched band on the 10 dB return loss condition is overlapped with wanted UWB operating frequency, i.e., the bandwidth of the notched band is unsatisfactory for UWB applications [19], [20].

Previous literatures have mainly focused on the band-notched UWB antenna for wide operating bandwidth and band-notched performance. The band-notched performance in these literatures could utilize three observed criteria to estimate notched band antenna performance, i.e., gain suppression, bandwidth and roll-off rate (frequency selectivity) of the notched band. These criteria strongly relate to the structure and quality factor of the resonator [18]–[20]. According to our knowledge and experiments, the resonator position at the antenna should be included in the notched-band antenna design because it is also related to notched band performance. Hence, the quality factor and resonator position can be accommodated simultaneously to improve the controlled ability of the notched band.

To investigate notched band performance, the proposed antenna consists of a fork-shaped antenna, an open-looped resonator with a high quality factor and two taped-lines. The fork-

Manuscript received January 16, 2009; revised October 01, 2009; accepted October 27, 2009. Date of publication March 29, 2010; date of current version June 03, 2010. This work was supported by the National Science Council, R.O.C., under Grant NSC 97-2219-E-009-012.

The authors are with the Department of Communication Engineering, Taiwan National Chiao Tung University, Hsinchu, Taiwan 300, R.O.C. (e-mail: sungjungwu.cm96g@nctu.edu.tw).

Digital Object Identifier 10.1109/TAP.2010.2046839

shaped antenna is designed for wide operating range. The proposed resonator is placed at the center of the fork-shaped antenna, creating the 5-GHz notched band. Using this arrangement, this work emphasizes the resonator effects. The proposed antenna also shows good performance, such as fast roll-off rate of return loss, good gain suppression ability and narrow notched bandwidth at the notched band.

Section II presents the geometry and design concept of the proposed antenna and discusses important parameters for the fork-shaped antenna and band-notched performance. Section III shows the equivalent circuit model as a simple way to estimate the notched frequency of the proposed antenna. The calculated antenna input impedance using the proposed circuit mode agrees with the full-wave simulation data. Section IV further examines the gain frequency response and group delay of the proposed antenna. Finally, Section V draws conclusions.

II. Antenna Configuration and Performance

A. Antenna Configuration and Performance

Fig. 1 shows the geometry of the proposed antenna consisting of the fork-shaped antenna and the proposed resonator. The wide operating bandwidth of the fork-shaped antenna is mainly determined by three parameters, i.e., L_1, L_2 and W_1. The lowest frequency is determined by (1) to (3) and the tapered profile of the antenna structure is described by (4). α is the angle between the radiator and the ground plane

$$f_l \approx \frac{c}{\sqrt{\varepsilon_{\text{eff}}} \cdot L_l} \tag{1}$$

$$L_l = L_1 + \sqrt{L_2^2 + W_1^2} \approx \frac{\lambda_l}{4} \tag{2}$$

$$\varepsilon_{\text{eff}} = \frac{\varepsilon_r + 1}{2} \tag{3}$$

$$\alpha = \tan^{-1}(L_2/W_1) \tag{4}$$

where L_l is the estimated longest current path along the outer radiating strip, approximated as a quarter of the length at the lowest frequency. The c and ε_{eff} are the speed of light and the approximated effective dielectric constant, respectively. The performance of the fork-shaped antenna at the UWB high band is related to α. Here, the UWB high band refers to the optional band from 5.85 to 10.65 GHz whereas the UWB low band represents the mandatory band from 3.1 to 5.1 GHz [1], [21]. In our experiments, α should be 0.4–0.6 for better return loss level at the UWB high band.

According to simulated current distributions of the planar monopole antenna, the current on the metal plate is inherently concentrated along the outer edges of the radiating plate, especially for the UWB low band. Based on this phenomenon, the resonator position at the interior of the antenna not only realizes a band-notched characteristic, but also preserves nearly the original characteristic of the antenna. The cutting triangular area, 0.5×3.5 mm $\times$ 14 mm, is applied here to place the proposed resonator.

To achieve the band-notched property, the proposed resonator is symmetric around its centerline and consists of one open-looped resonator and two tapped lines as shown in Fig. 1(b). The open-looped resonator is realized by folding back a half wavelength straight strip to form a pair of coupled lines. The coupled lines are connected together at one end. The total length of the coupled lines, $2 * L_5 + c$, approximates one-quarter wavelength. The current work uses the tapped-line to connect the proposed open-looped resonator and the fork-shaped antenna. The proposed resonator causes high input impedance level and impedance mismatching at the proposed antenna in the notched band.

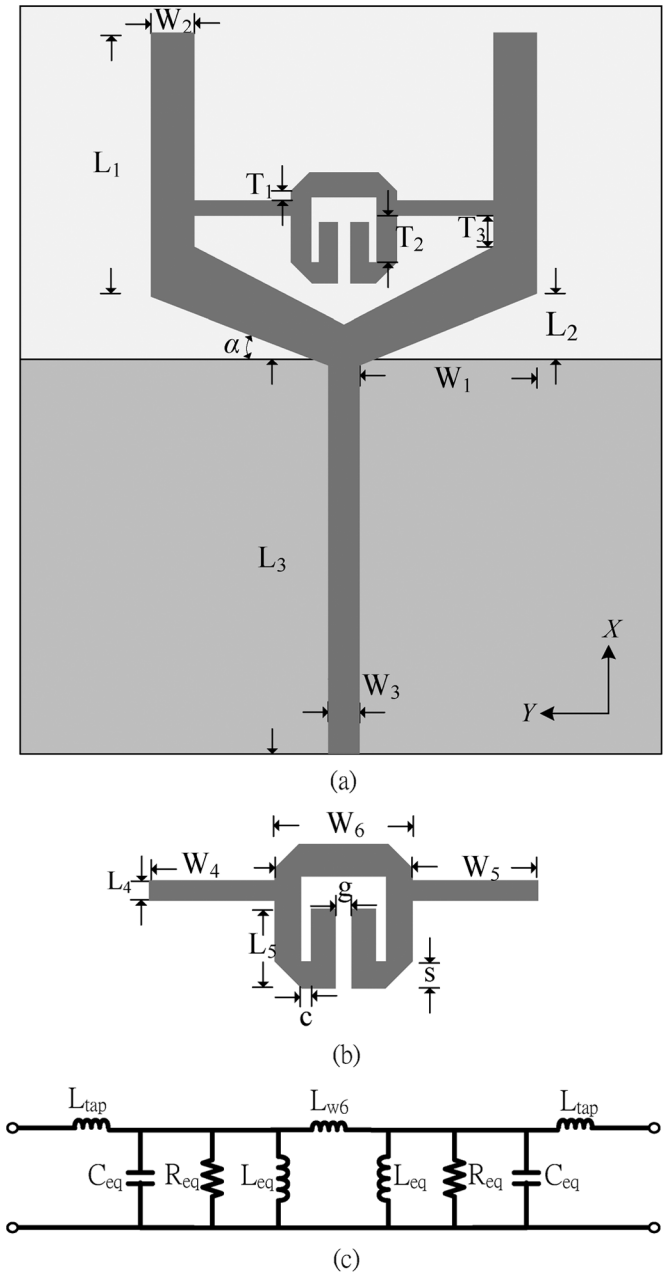

Fig. 1. Configuration of the proposed antenna. (a) Top view. (b) Proposed resonator. (c) Schematic equivalent circuit model of proposed resonator.

Conceptually, the proposed resonator can be represented by the schematic equivalent circuit model shown in Fig. 1(c), in which each coupled line and the strip of W_6 can be represented

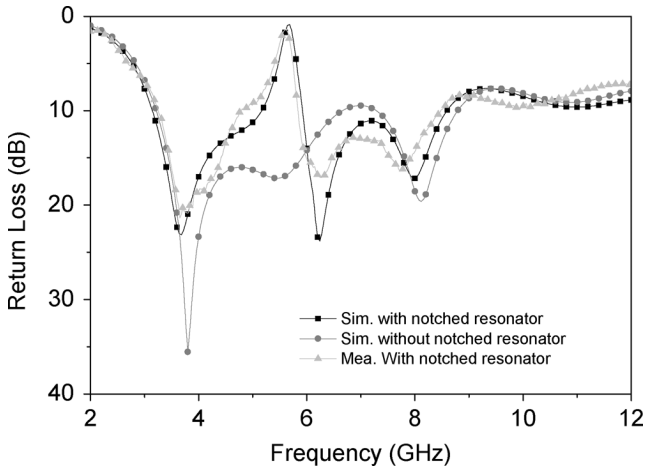

Fig. 2. Measured and simulated return loss of proposed antenna.

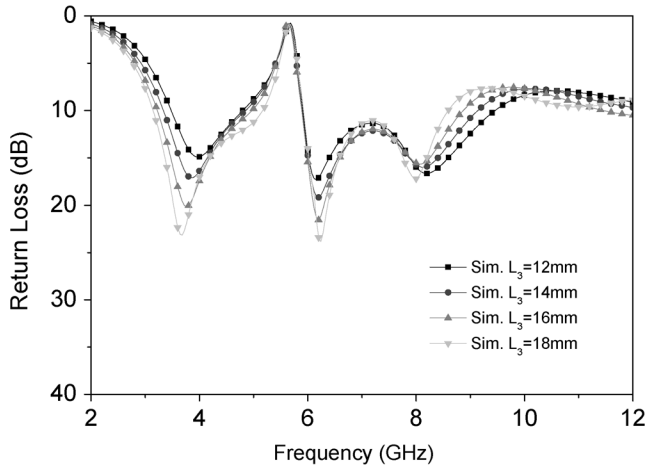

Fig. 3. Simulated return loss of various ground plane sizes.

by a lumped parallel lossy RLC circuit and inductive load, respectively. The tapped-line is treated as the inductive loads and capacitive loads. The capacitive coupling between two folded strips is ignored in Fig. 1(c). The resonant frequency of the proposed resonator can be readily controlled by adjusting the equivalent inductance and capacitance values. It is noted that the proposed resonator is operated in inhomogeneous media without background plane. Thus, the proposed resonator neither supports the TEM mode nor forms the microstrip line resonator. Section III discusses the analysis and the simplified equivalent circuit model.

The antenna was fabricated on a 35 mm $\times$ 30 mm $\times$ 0.769 mm Rogers RO4350 substrate with dielectric constant $\varepsilon_{\mathrm{r}} = 3.48$ and loss tangent = 0.004 at 10 GHz. The final design parameters are $\mathrm{W}_1 = 8.15$ mm, $\mathrm{W}_2 = 2$ mm, $\mathrm{W}_3 = 1.65$ mm, $\mathrm{W}_4 = 4.5$ mm, $\mathrm{W}_5 = 4.5$ mm, $\mathrm{W}_6 = 5$ mm, $\mathrm{L}_1 = 12.7$ mm, $\mathrm{L}_2 = 3.3$ mm, $\mathrm{L}_3 = 18$ mm, $\mathrm{L}_4 = 0.4$ mm, $\mathrm{L}_5 = 3$ mm, $\mathrm{T}_1 = 0.4$ mm, $\mathrm{T}_2 = 2.2$ mm, $\mathrm{T}_3 = 1.5$ mm, $\mathrm{c} = 0.3$ mm, $\mathrm{g} = 0.4$ mm, $\mathrm{s} = 1$ mm and $\mathrm{H} = 0.769$ mm.

Fig. 2 shows the simulated and measured return losses. The simulation was performed using Ansoft HFSS 9.2 while the measurement was taken by an Agilent E8362B performance network analyzer. The measured result agrees with the simulated result. The proposed resonator only slightly interferes with the return loss of the fork-shaped antenna except within the notched band. Fig. 2 also shows the simulated result of the antenna without the proposed resonator, evidencing that the desired band notched property is introduced by the proposed resonator. The notched band reveals the narrow bandwidth and the fast roll-off rate due to the high quality factor and the appropriate position of the resonator.

In general, the ground plane can be treated as part of a small antenna. In this work, it is necessary to discuss the effect of the ground plane. Fig. 3 shows the simulated return loss of various ground plane sizes. Observations show that the bandwidth of the UWB low band becomes significantly wider as L_3 changes from 12 mm to 18 mm but both the bandwidth of UWB high band and the return loss level of the notched band remain practically unchanged. According to this phenomenon, the larger ground size is proportional to the bandwidth at the UWB low band.

The antenna radiation patterns are measured in a 7.0 m $\times$ 3.6 m $\times$ 3.0 m anechoic chamber with an Agilent E8362B network analyzer along with NSI2000 far-field measurement software. Fig. 4 shows the measured radiation patterns in yz-, xz- and xy-planes at 4.5 and 8.5 GHz. The measured patterns agree with the simulated patterns. Referring to Fig. 4(a), the co-polarization patterns are probably omni-directional shaped. The cross-polarization level rises considerably as frequency increases. The cross-polarization level is comparable to the co-polarization level in the yz-plane. In Figs. 4(b) and (c), the co-polarization patterns are the roughly dumbbell-like shaped and the cross-polarization levels are generally much lower than co-polarization levels. The discrepancies of cross-polarization in xy-plane and yz-plane can be attributed to the interference of the coaxial cable and the absorber.

B. Effect of Resonator on Notched Bands

To comprehend the effect of the proposed resonator, this subsection discusses the geometric parameters of the proposed resonator along with the fork-shaped antenna. The following discussions evaluate band-notched performance by the bandwidth, roll-off rate and return loss level of the notched band.

Fig. 5 shows the simulated return loss of various folded lengths of the resonator. The folded length of the open-looped resonator is the dominated element on the notched band. As shown in Fig. 1(c), the folded length of the resonator, $2 * \mathrm{L}_5 + \mathrm{c}$, preliminarily determines the values of the parallel RLC circuit. In the meantime, the resonant frequency of the resonator is principally controlled by adjusting the values of the parallel RLC circuit. As the folded strip length becomes longer, the amount of capacitive load of the parallel RLC circuit increases accordingly. The center frequency of the notched band is simply in reverse proportion to the folded length of the resonator. Simultaneously, the bandwidth and return loss level retain their original value.

Fig. 6 shows the simulated return loss of various positions of the tapped-line. The position of the tapped line is the feeding

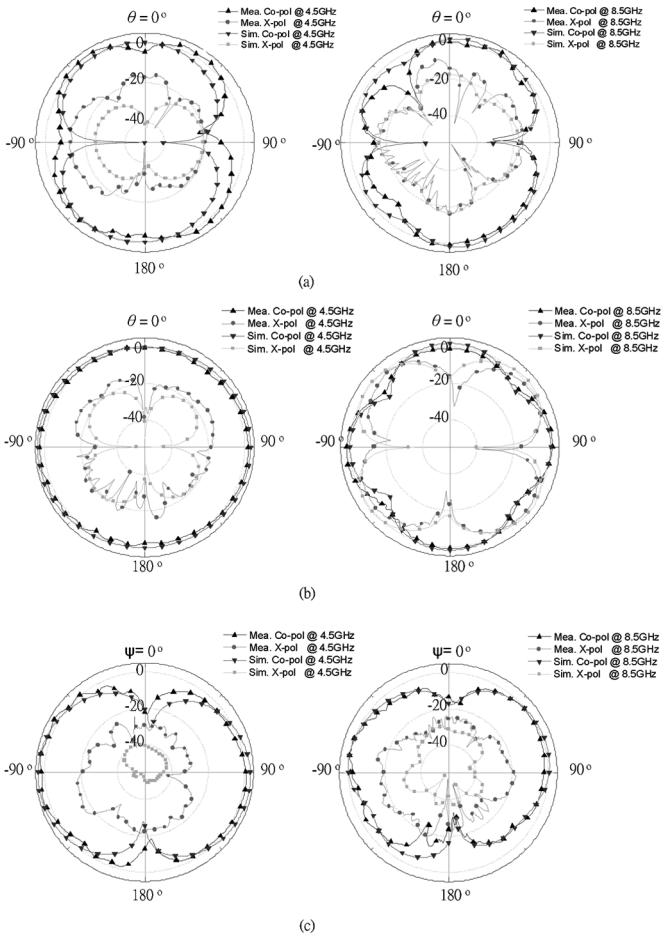

Fig. 4. Measured and Simulated radiation patterns at (a) yz-plane. (b) xz-plane. (c) xy-plane. (Unit:dBi)

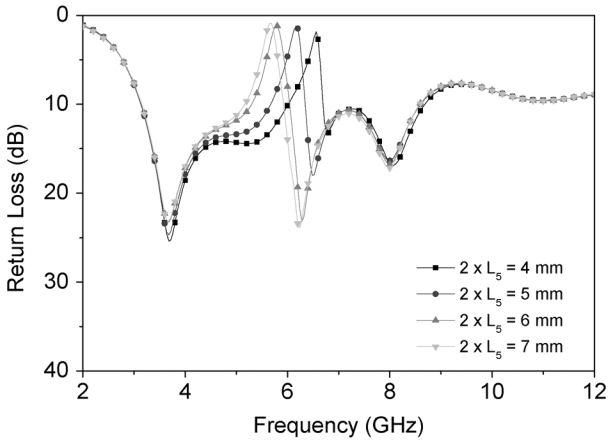

Fig. 5. Simulated return loss of various folded lengths of the resonator.

input of the resonator. In this case, the position of the tapped-line moves vertically while the position of the whole open-looped resonator at the antenna is fixed. In this arrangement, the center notched frequency varies from 5.24 GHz to 6.46 GHz as T_1 and T_2 respectively changes from 0.0 and 2.6 mm to 2.4 and 0.2 mm at the fixed T_3. The notched frequency shifts over a 1.2 GHz range as the tapped-line moves several millimeters. The result is different from the general filter design concept where

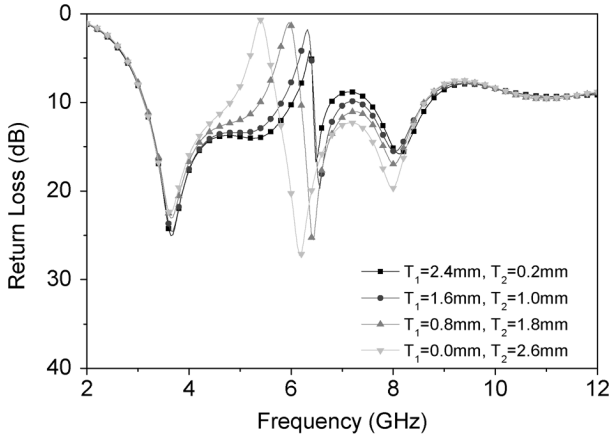

Fig. 6. Simulated return loss of various positions of the tapped-line.

the position of the tapped-line cannot dominate the resonant frequency. To explain this phenomenon, the current study employed an equivalent circuit model of the resonator shown in Section III. According to the simulated results of the equivalent circuit model, the resonant frequency only shifts around 0.2 GHz as the position of the tapped line changes in same condition. This implies a certain degree of dependency between the two situations, i.e., the resonator with ground plane and the resonator without ground plane. In the former situation, the resonator supports the quasi-TEM mode. Hence, the feeding position of the resonator cannot dominate the resonant frequency. In the latter situation, resonant frequency is easily influenced by changing the resonator input because the resonator is placed in the antenna/radiator without the ground plane.

Fig. 7 shows the simulated return loss according to various vertical positions of the resonator at the antenna, i.e., various values of T_3 while T_1, T_2, W_4 and W_5 are fixed. Here, the proposed resonator moves along the x-direction. The center frequency and the return loss level of the notched band slightly changes as T_3 changes from 1.8 mm to 7.8 mm, whereas the bandwidth of the notched band is significantly larger as the resonator is placed near the end of the fork-shaped antenna. In this case, since the proposed resonator structure is not changed, the unload quality factor of the proposed resonator or each component of Fig. 1(c) retains its original value. This study considers the external quality factor of the resonator when the resonator cooperates with the radiator/antenna. Fig. 7 implies that when the resonator is placed near the end of the fork-shaped antenna, the external quality factor becomes lower and the bandwidth of the notched band becomes wider simultaneously.

Fig. 8 shows the simulated return loss according to horizontal positions of the resonator at the antenna, i.e., various values of W_4 and W_5 at fixed T_1, T_2 and T_3. Different from Fig. 7, the proposed resonator moves along the y-direction. Referring to Fig. 1(c), L_{tap1} is not equal to L_{tap2} because W_4 is not equal to W_5. When the proposed antenna becomes non-symmetrical, the notched band moves farther apart and splits into two individual notched bands whose peak values are -1.2 dB at 5.56 GHz and -3.2 dB at 6.48 GHz when $W_4 = 2$ mm and $W_5 = 7$ mm, and are -2.91 dB at 5.4 GHz and -1.7 dB at 6.08 GHz when $W_4 = 3$ mm and $W_5 = 6$ mm, respectively. Fig. 8 shows that the

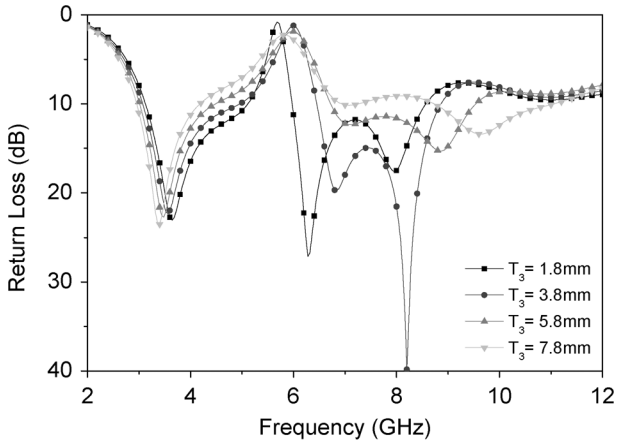

Fig. 7. Simulated return loss according to various vertical position of resonator at the antenna.

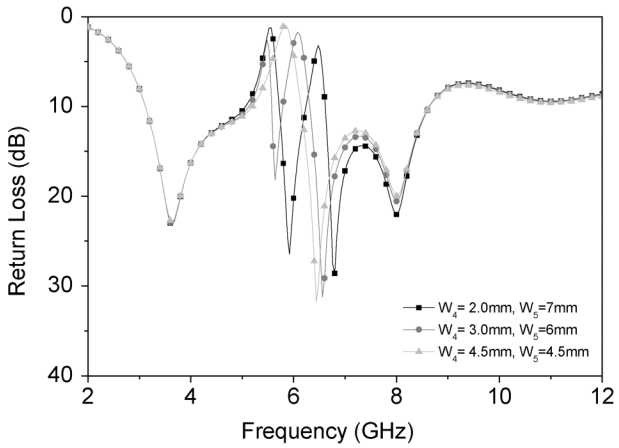

Fig. 8. Simulated return loss according to various horizontal positions of resonator at the antenna.

proposed resonator can be treated as two sub-resonators, where each sub-resonator is formed by a tapped-line and a folded strip of the open-looped resonator. The notched frequencies of the proposed antenna depend on the structure of each sub-resonator.

III. The Equivalent Circuit Model

Conceptually, the schematic equivalent circuit model shown in Fig. 1(c) represents the proposed resonator. The inductive and capacitive loads explain the band-notched behaviors at the notched band. However, it is difficult for band-notched antenna modeling using the schematic equivalent circuit model to obtain accurate values of each component. To tackle this problem, this section proposes the simplified equivalent circuit model to explain complex resonant behaviors.

This work first extracts the impedance characteristic of the proposed resonator shown in Fig. 9(a). Here, the dimension of each ground plane is 8×20 mm^2 and the two delta sources excite at each node interface of the proposed resonator at the Ref plane. The proposed resonator in the fork-shaped antenna is actually floating. Therefore, during the extracting process shown in Fig. 9(a), the proposed resonator is placed at the RO4350 substrate without ground plane to accompany the actual operating mechanism.

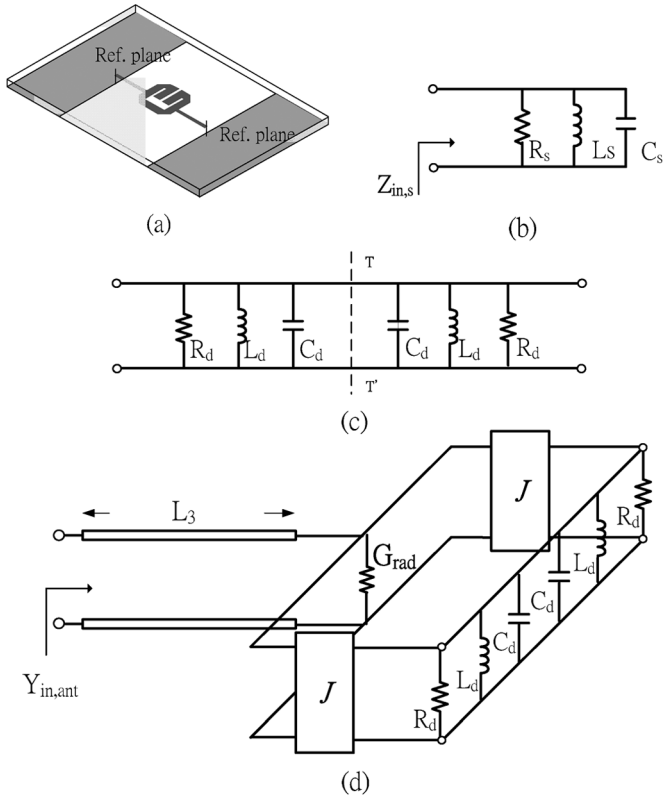

Fig. 9. (a) Exacting structure of the proposed resonator. (b) One-port lump equivalent circuit network of the proposed resonator. (c) Two-port lump equivalent circuit network of the proposed resonator. (d) Simplified equivalent circuit model of the proposed antenna.

To transfer the proposed resonator to the equivalent lumped circuit model, the procedure of the equivalent lumped circuit model shown in Fig. 9(b) and (c) can be accounted for using the filter design theory in [[22], Chap 6–8]. Using the HFSS simulation, the Z-parameters of the proposed resonator can be easily achieved and can transfer into a one-port lumped equivalent parallel resonant as shown in Fig. 9(b) with

$$L_s = \frac{R_s}{2\pi f_c * Q_s} \tag{5}$$

$$C_s = \frac{1}{(2\pi f_c)^2 L_s} \tag{6}$$

$$Q_s = \frac{f_c}{f_u - f_l} = \frac{1}{\mathrm{FBW}} \tag{7}$$

where FBW is the fractional bandwidth. f_u and f_l are frequencies as the input impedance magnitude of the one-port resonant network is respectively 0.707 times the maximum magnitude of the one-port network. f_c is the center resonant frequency of the resonator. $\mathrm{R_s}$ is the real part of the impedance of the one-port network at the center frequency. $\mathrm{L_s}$ and $\mathrm{C_s}$ are the inductance and capacitance of the one-port network, respectively [21]. Because the resonator is symmetrical, the one-port resonant network can separate into the symmetrical two-port resonant network as shown in Fig. 9(c). The T-T' line is a symmetrical plane.

TABLE I
EXTRACTED VALUES OF THE RESONATOR PARAMETERS AND J INVERTER

f_c	f_l	f_u
5.4GHz	5.24GHz	5.52GHz
R_d	C_d	L_d
1222ohm	0.467pF	1.85nH
Q_d	J-inverter	G_{rad}
9.64	0.057mho	0.02 mho

Here, we define two-port network elements, $\mathrm{Q_d}$, $\mathrm{L_d}$, $\mathrm{C_d}$ and $\mathrm{R_d}$, as

$$Q_d = \frac{Q_s}{2} \tag{8}$$
$$L_d = 2L_s \tag{9}$$
$$C_d = \frac{C_s}{2} \tag{10}$$
$$R_d = 2R_s. \tag{11}$$

Note that $\mathrm{R_d}$ is the real part of impedance of the two-port network and is $2\mathrm{R_s}$ to keep the real part of implement of the two-port network equal to that of the one-port network. $\mathrm{R_s}$ or $\mathrm{R_d}$ in the lumped circuit model represents the amount of conductor and dielectric loss, not radiation loss. Fig. 9(c) presents the proposed resonator with two node interfaces by a two-port lumped circuit model.

In the modeling process, the metal strip is regarded as the high impedance line with a length of $\mathrm{T_3} + (\mathrm{W_1} + L_2)^{0.5}$, which is approximately one-quarter wavelength of the notched band. Here, the metal strip is between the proposed resonator and the feeding microstrip line. Hence, this metal strip behaves quite similarly to a quarter-wavelength transformer, and can be therefore modeled as a pair of J-inverters [21], [22]. The values of the J-inverter are determined by the characteristic admittance of the feeding microstrip line and the real-part admittance of the equivalent resonant circuit. $\mathrm{G_{rad}}$ stands for a constant radiation conductance and accounts for the wideband nature of the antenna. Finally, a simplified equivalent circuit model presents the proposed antenna as shown in Fig. 9(d). The extracted values of resonator parameters are summarized in Table I and $\mathrm{Y_{in,\ ant}}$ is the input admittance of the antenna given by

$$\mathrm{Y_{in,ant}} = \mathrm{G_{rad}} + \frac{2\mathrm{J}^2}{\frac{1}{\mathrm{R_d}} + j\omega\mathrm{C_d} + \frac{1}{j\omega\mathrm{L_d}}}. \tag{12}$$

Fig. 10 shows the simulated impedance of the proposed resonator and the simulated admittance of the proposed antenna, respectively. Reasonable agreement exists between the results of the HFSS simulation and the simplified equivalent circuit model. The discrepancy between the curves mostly attributes to the simplistic modeling of the resonator and the J-inverter. The results, in terms of a simplified equivalent circuit with higher quality factor, reasonably explain the narrower bandwidth of

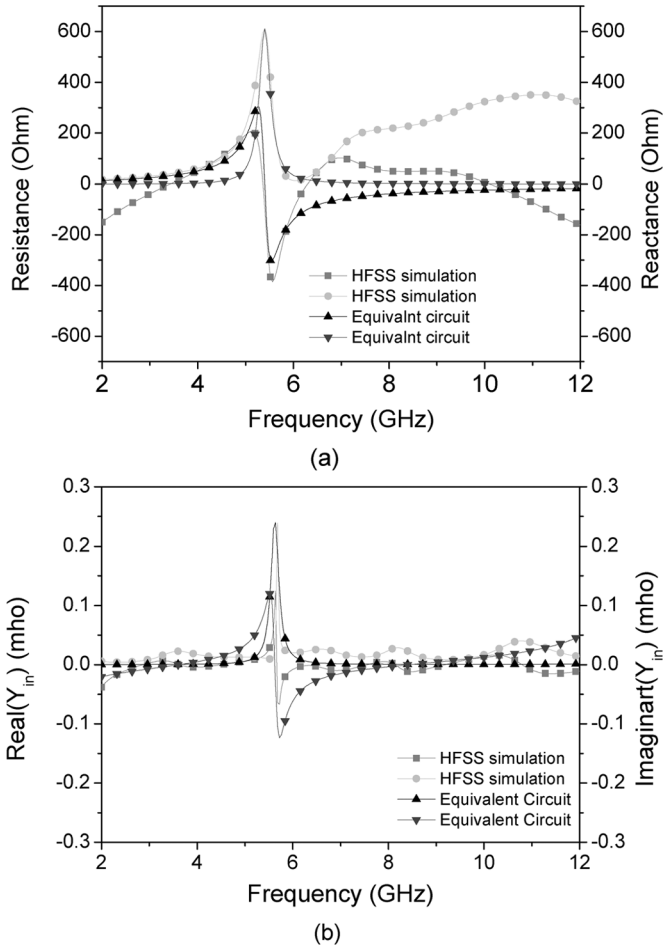

Fig. 10. Compared results between HFSS and the simplified equivalent circuit. (a) Simulated impedance of the resonator. (b) Simulated admittance of the proposed antenna.

frequency gain response in Section IV. Despite some inaccuracy in the simplified equivalent circuit model, the results still provide valuable information of antenna behavior.

IV. MEASURED GAIN RESPONSE AND GROUP DELAY

In measuring antenna gain frequency response, the EMCO 3115 double-ridge horn antenna with a constant group delay of 630 ps is used as a reference antenna for calibration. Fig. 11 illustrates the measured gain frequency responses in the yz-plane at eight angles, ranged from -180° to 180° with 45° interval. The gain response of the proposed antenna is quite flat from 3.1 to 10.6 GHz except at the notched band. According to Fig. 11, the range of gain suppression is from 15 dB to 35 dB within these eight angles at the target notched band. Although the notched band slightly shifts at $\theta = 90^\circ$ and at $\theta = -90^\circ$, it remains within the range of the target notched band. The notched frequencies are quite similar at the observation angles. The notched bandwidth is significantly narrower due to the fast roll-off rate and high level of return loss at the notched band. The distance between the referenced antenna and the proposed antenna is 3.4 m. In the UWB system, the constant group delay response is required. Fig. 12 presents the measured group delay of the proposed antenna. Except at the notched band, group

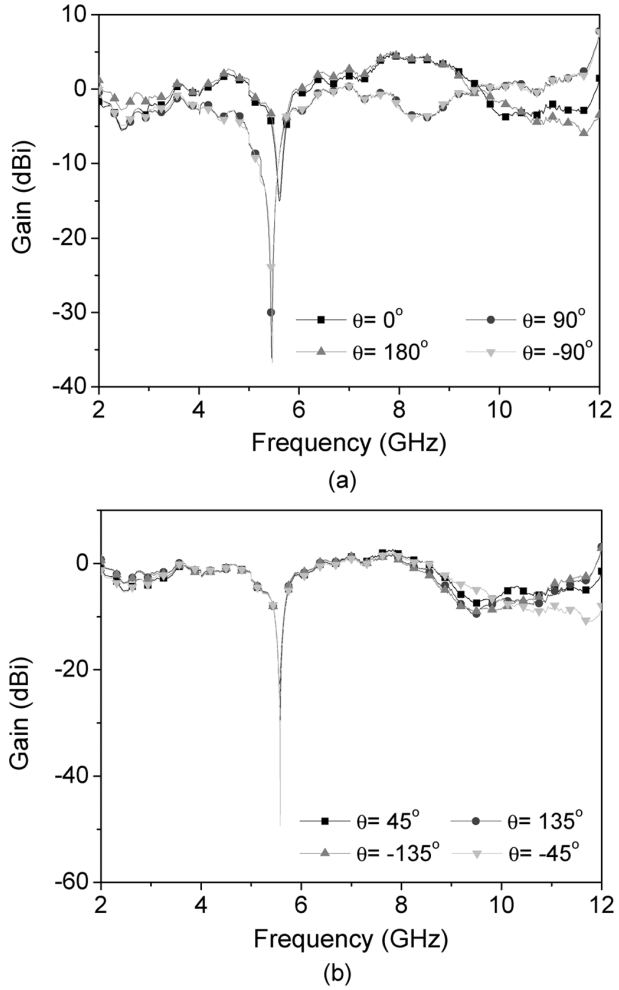

Fig. 11. Measured gain response of the proposed antenna. (a) $\theta = 0°$, $\theta = 90°$, $\theta = 180°$, $\theta = -90°$. (b) $\theta = 45°$, $\theta = 135°$, $\theta = -135°$, $\theta = -45°$.

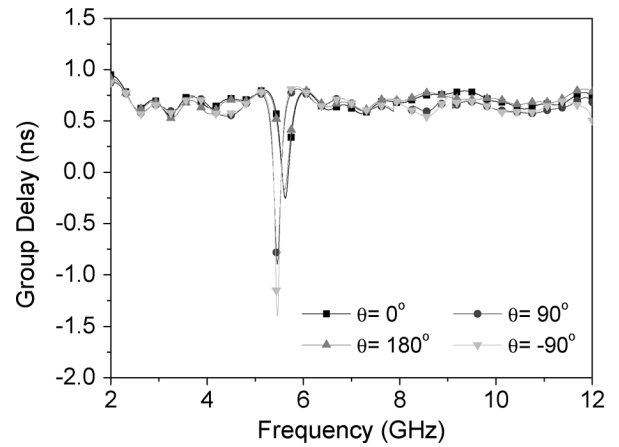

Fig. 12. Measured group delay of the proposed antenna.

delay variation over the 3.1 to 10.6 GHz is less than 130 ps with average of 718 ps as the spatial angle varies. Figs. 11 and 12 show that the proposed antenna has good time/frequency characteristics and a small pulse distortion over the UWB operated band.

V. Conclusion

This paper proposes and analyzes a novel band-notched monopole ultrawideband antenna. By applying an open-looped resonator, the antenna shows a narrower bandwidth and high return loss level as well as good gain suppression ability at the desired notched band. The parameter studies of the proposed antenna provide brief guidelines for a band-notched antenna design using the similar monopole antenna and resonator. This study investigates these parameters in terms of the relationship between the fork-shaped antenna and the open-looped resonator. The simplified equivalent circuit model explains the rather complicated resonant behavior of the proposed antenna. The calculated antenna input admittance using the simplified equivalent circuit model agrees with the HFSS simulated result. Evaluations of return loss, radiation patterns, gain responses, and group delay confirm the antenna performance. These features of the proposed antenna demonstrate that the proposed antenna is suitable for UWB communicational applications and prevents interference from the WLAN system.

Acknowledgment

The authors would like to thank Wireless Communication and Electromagnetism Application Lab of the National Taiwan University of Science and Technology, Taiwan, ROC., for supporting the far field measurement

References

[1] UWB, Forum Homepage [Online]. Available: http://www.uwbforum
[2] Task Group 3a Homepage [Online]. Available: http://www.ieee802.org/15/pub/TG3a.html
[3] J. S. McLean, H. Foltz, and R. Sutton, "Pattern descriptors for UWB antennas," *IEEE Trans. Antennas Propag.*, vol. 53, pp. 553–559, Jan. 2005.
[4] S. B. T. Wang, A. M. Niknejad, and R. W. Brodersen, "Circuit modeling methodology for UWB omnidirectional small antennas," *IEEE J. Select. Areas Commun.*, vol. 24, no. 4, pp. 871–877, 2006.
[5] A. M. Abbosh and M. E. Bialkowski, "Design of ultrawideband planar monopole antennas of circular and elliptical shape," *IEEE Trans. Antennas Propag.*, vol. 56, no. 1, pp. 17–23, Jan. 2008.
[6] Z. N. Chen, T. S. P. See, and X. Qing, "Small printed ultrawideband antenna with reduced ground plane effect," *IEEE Trans. Antennas Propag.*, vol. 55, no. 2, pp. 383–388, Feb. 2007.
[7] C. Shi, P. Hallbjorner, and A. Rydberg, "Printed slot planar inverted cone antenna for ultrawideband applications," *IEEE Antennas Wireless Propag. Lett.*, vol. 7, pp. 18–21, 2008.
[8] T. G. Ma and S. K. Jeng, "Planar miniature tapered-slot-fed annular slot antennas for ultrawideband radios," *IEEE Trans. Antennas Propag.*, vol. 53, pp. 1194–1202, Mar. 2005.
[9] X. N. Low, Z. N. Chen, and W. K. Toh, "Ultrawideband suspended plate antenna with enhance impedance and radiation performance," *IEEE Trans. Antennas Propag.*, vol. 56, no. 8, pp. 2490–2495, Aug. 2008.
[10] C. D. Zhao, "Analysis on the properties of a coupled planar dipole UWB antenna," *IEEE Antennas Wireless Propag. Lett.*, vol. 3, pp. 317–320, 2004.
[11] J. Qiu, Z. Du, J. Lu, and K. Gong, "A planar monopole antenna design with band-notched characteristic," *IEEE Trans. Antennas Propag.*, vol. 54, no. 1, pp. 288–292, Jan. 2006.
[12] W. S. Lee, W. G. Lim, and J. W. Yu, "Multiple band-notched planar monopole antenna for multiband wireless systems," *IEEE Microwave Wireless Compon. Lett.*, vol. 15, pp. 576–578, Sept. 2005.
[13] Y. J. Cho, K. H. Kim, D. H. Choi, S. S. Lee, and S. O. Park, "A miniature UWB planar monopole antenna with 5-GHz band-rejection filter and the time-domain characteristics," *IEEE Trans. Antennas Propag.*, vol. 54, pp. 1453–1460, May 2006.

[14] T. Dissanayake and K. P. Esselle, "Predication of the notch frequency of slot loaded printed UWB antennas," *IEEE Trans. Antennas Propag.*, vol. 55, no. 11, pp. 3320–3325, Nov. 2007.
[15] Y. Lin and K. J. Hung, "Compact ultrawideband rectangular aperture antenna and band-notched designs," *IEEE Trans. Antennas Propag.*, vol. 54, pp. 3075–3081, Nov. 2006.
[16] K. H. Kim and S. O. Park, "Analysis of the small band-rejected antenna with the parasitic strip for UWB," *IEEE Trans. Antennas Propag.*, vol. 54, pp. 1688–1692, June 2006.
[17] S. W. Qu, J. L. Li, and Q. Xue, "A band-notched ultrawideband printed monopole antenna," *IEEE Antennas Wireless Propag. Lett.*, vol. 5, pp. 495–498, 2006.
[18] R. Zaker, C. Ghobadi, and J. Nourinia, "Novel modified UWB planar monopole antenna with variable frequency band-notch function," *IEEE Antennas Wireless Propag. Lett.*, vol. 7, pp. 112–114, 2008.
[19] T. G. Ma and S. J. Wu, "Ultrawideband band-notched U-shape folded monopole antenna and its radiation characteristics," in *Ultra-Wideband Short Pulse Electromagnetics 8*. Berlin, Germany: Springer Publisher, 2007, pp. 49–56.
[20] C.-Y. Hong, C.-W. Ling, I.-Y. Tran, and S.-J. Chung, "Design of a planar ultrawideband antenna with a new band-notch structure," *IEEE Trans. Antennas Propag.*, vol. 55, no. 12, pp. 3391–3397, Dec. 2007.
[21] T. G. Ma and S. J. Wu, "Ultrawideband band-notched folded strip monopole antenna," *IEEE Trans. Antennas Propag.*, vol. 55, pp. 2473–2479, Sept. 2007.
[22] J. S. Hong and M. J. Lancaster, *Microstrip Filter for RF/Microwave Application*. New York: Wiley, 2001.

Sung-Jung Wu was born in Taipei, Taiwan, R.O.C., in 1980. He received the B.S. degree in electrical engineering from TamKang University (TKU), Taipei, in 2004, and the M.S. degree in electrical engineering from National Taiwan University of Science and Technology (NTUST), Taipei, in 2007. He is currently working toward the Ph.D. degree at National Chiao Tung University, Hsinchu, Taiwan.

He worked with the Foxconn Technology Co., Ltd., Taiwan, and Sunplus Technology Co., Hsinchu, for RF circuit design in 2004–2006 and 2006–2008 respectively. His research interests include mobile antenna designs, RFID tag antenna designs, and UWB antenna designs, reconfigurable antenna design.

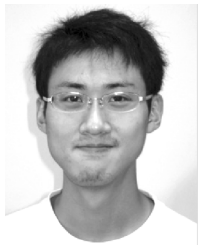

Keng-Hsien Chen was born in Taipei, Taiwan, R.O.C., in 1986. He received the B.S. degree in electrical engineering from National Taiwan Ocean University, Keelung, Taiwan, in 2008. He is currently working toward the M.S. degree at National Chiao Tung University, Hsinchu, Taiwan.

His current research interests include microwave antenna and circuits, reconfigurable antennas, and electromagnetic compatibility.

Cheng-Hung Kang was born in Yilan, Taiwan, R.O.C., in 1986. He received the B.S. degree in communication engineering from National Chiao Tung University, Hsinchu, R.O.C., in 2008, where he is currently working toward the M.S. degree.

His research interests include antenna designs, UWB antenna and passive circuit designs.

Jenn-Hwan Tarng (S'85–M'89–SM'06) received Ph.D. degree in electrical engineering from Pennsylvania State University, University Park, in 1989.

After obtaining the Ph.D. degree, he joined the Faculty of National Chiao-Tung University (NCTU), Hsin-Chu, Taiwan, R.O.C., where he now holds a position as Professor in the Department of Electrical Engineering. During 2003–2005, he was the Chairman of the Communication Engineering Department and Director of ARTS (Advanced Radio Technology and Systems) Center, NCTU, and then he was invited (on leave) as Chair Professor and Dean of Engineering College, Chung-Hua University from 2005–2007. From 2007–2009, he was also on leave and acted as the General Director of ISTC (Identification and Security Technology Center) of ITRI (Industrial Technology Research Institute), Taiwan, ROC. In the center, he led more than 150 R&D engineers to develop advanced RF ID and physical security technologies and systems to enhance associated local industries global competition. His professional interests include radio propagation modeling and measurement, frequency management, antenna design, RF IC and EMI/EMC.